Supramolecular Morphology of Two-Step, Melt-Spun Poly(lactic acid) Fibers

John A. Cicero,[1] John R. Dorgan,[1] Jay Janzen,[1] James Garrett,[2] James Runt,[2] J. S. Lin[3]

[1]*Department of Chemical Engineering, Colorado School of Mines, Golden, Colorado 80401-1887*
[2]*Department of Materials Science and Engineering, Pennsylvania State University, University Park, Pennsylvania 16802*
[3]*Solid State Division, Oak Ridge National Laboratory, Oak Ridge, Tennessee 37831*

Received 7 December 2001; accepted 1 April 2002

ABSTRACT: Fibers of poly(lactic acid) produced by two-step melt spinning have been studied. The morphology is elucidated with respect to the thermal and mechanical properties of fibers produced at cold-draw ratios of 1–8. With atomic force microscopy and small-angle X-ray scattering, a fibrillar morphology is found, with microfibril diameters ranging from 30 to 60 nm. Shrinkage properties indicate that, with increasing draw ratio, the fibers undergo a transition from class 2 to class 1 within the classification proposed by Keller. A supramolecular model for the morphology of the fibers is presented that entails a highly oriented skin with a core consisting of microfibrils. The orientation of the crystalline blocks within the microfibrils is similar to what has been reported for nylon fibers. © 2002 Wiley Periodicals, Inc. J Appl Polym Sci 86: 2828–2838, 2002

Key words: fibers; melt; morphology

INTRODUCTION

The globalization of the industrial revolution brings pressing questions about the sustainability of this structure of the plastics industry. Reductions in embedded energy content are desirable from both economic and environmental perspectives. As the industrial world is becoming more focused on environmentally benign manufacturing, interest in plastics from renewable resources intensifies. A worldwide developmental effort is currently underway on poly(lactic acid) (PLA), a polyester that can degrade under appropriate conditions but that also can be manipulated to maintain a long service life under other conditions. The many advantages of PLA include (1) availability from renewable agricultural resources, such as corn; (2) reductions in carbon dioxide emissions in comparison with conventional commodity plastics; (3) improvement of farm economies; and (4) excellent processability. In addition to its biodegradability, PLA is readily broken down thermally or by hydrolysis. Cargill Dow is wasting no time: a production plant in Blair, NE, with an annual capacity of 300 million pounds, is in operation. Primary markets for PLA include packaging, film, and fibers.

From a scientific viewpoint, one of the most intriguing features of PLA is that the monomer possesses chirality. The lactide monomer may contain identical stereocenters (L:L) or enantiomeric stereocenters (L:D). Copolymers of various L:D compositions may be formed with different ratios of monomers. Generally, L units are present in greater amounts than D units. Because the D units can serve as defects in an L chain, fully amorphous materials can be made by the inclusion of relatively high D contents (>20%), whereas highly crystalline materials are obtained when the D content is low (<2%).

In the literature, several groups have reported the mechanical properties of solution-spun[1–5] and melt-spun[6–11] PLA fibers. Scanning electron microscopy was used by Yuan et al.,[11] Fambri and coworkers,[1,6] and Leenslag et al.[4] to examine the surface structure with attention paid to roughness and fracture surfaces. Other groups, such as Hoogsteen et al.[12] and Eling et al.,[7] used wide-angle X-ray scattering to examine the crystal structure. However, a comprehensive study of the supramolecular morphology of PLA fibers has not appeared in the open literature, and this is the aim of this work.

MATERIALS AND METHODS

The PLA resin used in this study was a 6200D standard staple-fiber grade provided by Cargill Dow (Minnetonka, MN) in the form of pellets. It had a 98:02

Correspondence to: J. R. Dorgan (jdorgan@mines.edu).
Contract grant sponsor: Agriculture Industries of the Future Program, Office of Industrial Technologies, U.S. Department of Energy; contract grant number: DE-FC07-99CH11010.

Journal of Applied Polymer Science, Vol. 86, 2828–2838 (2002)

ratio of L:D stereochemical centers. Gel permeation chromatography with light scattering detection indicated that the number-average and weight-average molecular weights were 47,600 and 98,500, respectively. Before processing, the pellets were dried by reading a 1-in.-thick layer in the bottom of a stainless steel pan, which was placed in a convection oven at 82°C overnight (ca. 14 h). Postdrying water concentrations were expected to be about 100 ppm.[13]

A two-step melt-spinning process was used to produce the fibers. The apparatus consisted of a Killion KL-125 single-screw extruder mated to a Killion monofilament line. In this study, the draw ratio (DR) is the cold-draw ratio, defined as the velocity of the fiber at the take-up winder divided by the velocity at the first godet. The first godet was kept at 60 ft/min, and the speed of the take-up winder was adjusted to provide DRs of 1–8.

Differential scanning calorimetry (DSC) scans were performed with a PerkinElmer DSC 7, which was calibrated with an indium standard before each set of analyses. Samples were prepared by fibers being cut into pieces 2–4 mm long, dried in a vacuum oven at 40°C overnight, and then placed into aluminum pans (ca. 10 mg per pan). The samples were scanned from 25 to 200°C at a rate of 15°C/min.

Dynamic mechanical thermal analysis (DMTA) was performed with a Rheometric Scientific ARES rheometer fitted with fiber fixtures. Each strand was chosen at random, and the diameter was obtained with an optical microscope in conjunction with LECO image analysis software. The gauge lengths were 32.5 mm. The fibers were loaded at room temperature with a prestrain of 3%. The temperature sweep was started at 30°C and ramped to 130°C at 2°C/min. A frequency of 1 Hz and a strain amplitude of 0.2% were used for all samples.

Five fibers from each DR were selected randomly for shrinkage in boiling water experiments. After the measurements of the initial lengths, the fibers were submerged in boiling water (the bath was at 93°C because of the high altitude) for 15 min. After removal from the bath, the length of each fiber was again measured. The shrinkage percentage was defined as

$$\text{Shrinkage (\%)} = \frac{l_0 - l_1}{l_0} \times 100\% \qquad (1)$$

where l_0 and l are the lengths of the original and shrunk fibers, respectively. Results were reported as the averages of five fibers for each DR.

The morphology of the PLA fibers was examined with atomic force microscopy (AFM) and small-angle X-ray scattering (SAXS). SAXS data were obtained at the Oak Ridge National Laboratory 10-m pinhole-collimated SAXS camera, with X-rays 0.154 nm in wavelength and a 20 cm × 20 cm two-dimensional proportional detector. The sample-to-detector distance was 5.12 m for all experiments. The fiber samples were carefully wrapped around an aluminum frame and mounted vertically.

To prepare each AFM sample, a razor blade was used to make a notch nearly parallel to the fiber axis. The fiber was then pulled apart longitudinally to reveal an unscratched inner surface. An approximately 1-cm-long section of the shed fiber was placed on a magnetic AFM disk with double-sided tape. A Digital Instruments NanoScope IIIa AFM instrument operating in the tapping mode (height and phase) was employed. A low scanning rate of 0.7 Hz was used for optimum accuracy. Typical amplitude set points ranged from 0.4 to 0.8 V. Silicon Nanoprobe tips with resonant frequencies near 330 kHz were used.

RESULTS AND DISCUSSION

A DSC thermogram of a sample with a DR of 6 is shown in Figure 1. The melting temperature (T_m) is defined here as the temperature at the maximum of the melting endotherm. The glass-transition temperature (T_g) is taken as the inflection point in the heat capacity change in the vicinity of 60°C. For all DRs, a small exothermic region, an effect of physical aging, immediately follows T_g. In some cases, particularly in samples in which crystallinity is low, a trough due to cold crystallization in DSC is seen approximately halfway between T_g and T_m. To account for this effect, the crystallinity percentage of the samples is determined by subtraction of the area of the recrystallization trough from the area under the melting endotherm and division by a value of 93.6 J/g for 100% crystalline PLA.[14] Furthermore, two melting peaks separated by a few degrees are seen in some cases; in such cases, the higher melting point is reported. In other cases, a distinct shoulder can be seen on the low-temperature side of the melting peak. Fambri et al.[6] and Mezghani and Spruiell[10] made similar observations.

Table I presents values for T_g, T_m, and crystallinity percentage for each DR. The temperature of the fiber during drawing in the radiant heating zone, derived from heat-transfer modeling,[15] is also included in the table. The fiber temperature plays a significant role in the development of the properties; Figure 2 shows how the crystallinity percentage depends on the DR and fiber temperature. It is clear that lower temperatures and higher DRs increase crystallinity. However, excessive drawing or insufficient temperatures result first in surface crazing and ultimately fracture during drawing. The Gibbs–Thomson equation relates the lamellar thickness to the melting temperature, allowing an estimation of the mean lamellar thickness from measured melting points:[16,17]

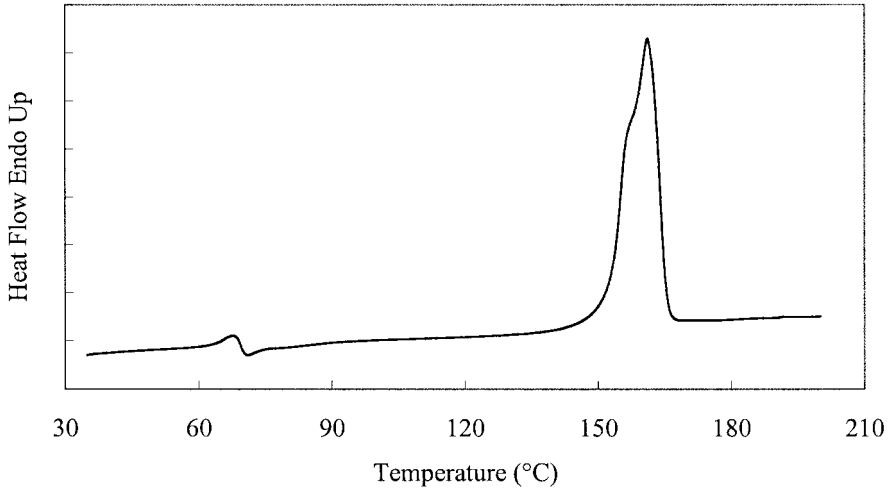

Figure 1 DSC thermogram of a fiber drawn to DR = 6.

$$L = \frac{2\sigma_e}{\Delta H_f(1 - T_m/T_m^o)} \quad (2)$$

where L is the lamellar thickness, σ_e is the surface free energy per unit area, ΔH_f is the melting enthalpy per unit volume of an infinite single crystal, T_m^o is the melting temperature of an infinite single crystal, and T_m is the observed melting temperature. For the purposes of this estimate, $\sigma_e = 48$ mJ/m^2, $\Delta H_f = 93.6$ J/g $= 1.16 \times 10^8$ J/m^3, and $T_m^o = 200$°C.[18] Calculations based on the highest observed T_m produce values for all fibers of 9–10 nm.

A typical DMTA plot, displaying the elastic modulus (E') and tan δ (E''/E') as functions of temperature, is shown in Figure 3. The mechanical glass transition is taken as the temperature of the maximum in tan δ. Below T_g, E' does not change much with temperature because the amorphous molecules are still essentially glassy. As soon as T_g is approached, however, the uncrystallized polymer chains begin to move, resulting in decreased stiffness. In fact, for low-DR fibers in which orientation of the chains is less developed, the samples relax beyond the prestrain at temperatures between T_g and 130°C, thereby terminating the test.

TABLE I
DSC Data and Fiber Temperature During Drawing for PLA Fibers

DR	T_g (°C)	T_m (°C)	Crystallinity (%)	Cold-draw temperature (°C)
1	61.7	162.2	0	93
2	61.9	165.1	0	86
3	63.5	164.0	32	82
4	65.5	161.9	24	77
5	67.0	160.6	34	75
6	67.7	161.2	47	73
7	70.2	162.1	49	72
8	68.7	162.9	51	71

T_g's obtained from DSC and DMTA are shown in Figure 4. The first point to note is that values increase with DR. Because the glass transition is associated with cooperative segmental motions of the amorphous molecules, it follows that if the molecular motions are inhibited, the temperature necessary to provide mobility will be higher than if the chains were unrestricted. Amorphous chains anchored by crystallites are restricted in their movements. Therefore, the trend of increasing T_g with DR coincides with increasing crystallinity, enhanced chain orientation, and restricted molecular mobility in the amorphous phase.

Although the thermally determined T_g values from DSC seem to increase somewhat smoothly with DR, the mechanically determined values from DMTA ex-

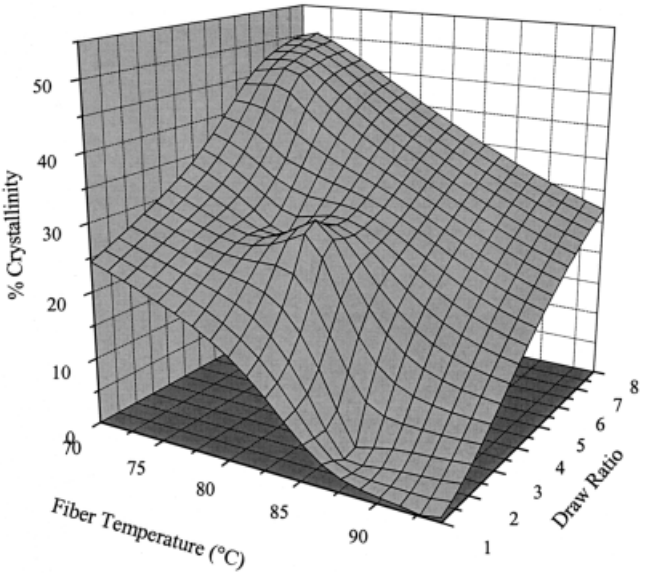

Figure 2 Three-dimensional plot showing the combined effects of stress and temperature on fiber crystallinity.

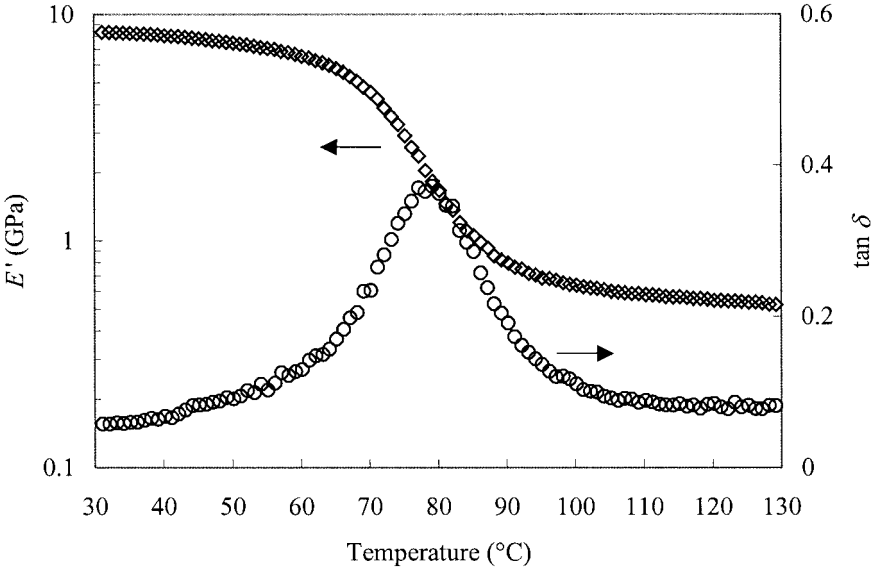

Figure 3 Typical DMTA plot of E' and tan δ versus temperature. T_g was taken at the maximum in tan δ.

hibit an abrupt jump of about 10°C from DR = 5 to DR = 6. This transition is also evident in a number of properties for the PLA fibers studied, notably fiber shrinkage.[15] Moreover, the T_g values obtained from DMTA are higher than those from DSC. The fibers studied with DSC are unconstrained and can relax before reaching T_g. Sub-T_g relaxation is inhibited for the DMTA experiment because the fibers are always slightly stressed. The confinement of the prestrain prevents, or at least slows down, relaxation.

Physical aging reduces free volume in the amorphous regions of semicrystalline polymers. This densification process results in increased stiffness. Figure 5 demonstrates the effect of physical aging on E' of a PLA fiber drawn to DR = 6 that was stored for 45 days before testing. The temperature is scanned up from 30 to 140°C and back down to 30°C at the same rate (2°C/min). During the heating portion of the scan, secondary crystallization or annealing occurs above T_g. The E' values for temperatures above T_g reported during the cooling portion are, therefore, higher than those in the same temperature range for the heating portion. However, heating to 140°C erases the physical aging history of the amorphous phase. Remarkably, the loss in E' due to erasing the physical aging overcomes the increase caused by secondary crystallization. The result is a lower E' below T_g, evident in Figure 5 at the low temperatures.

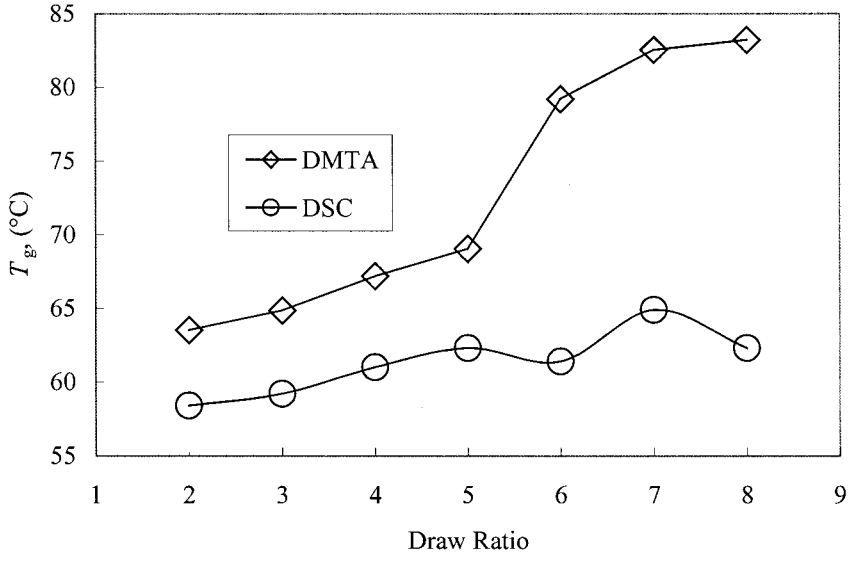

Figure 4 T_g versus the DR from DMTA and DSC analyses. Note the abrupt jump at DR = 5 for the mechanically determined value of T_g.

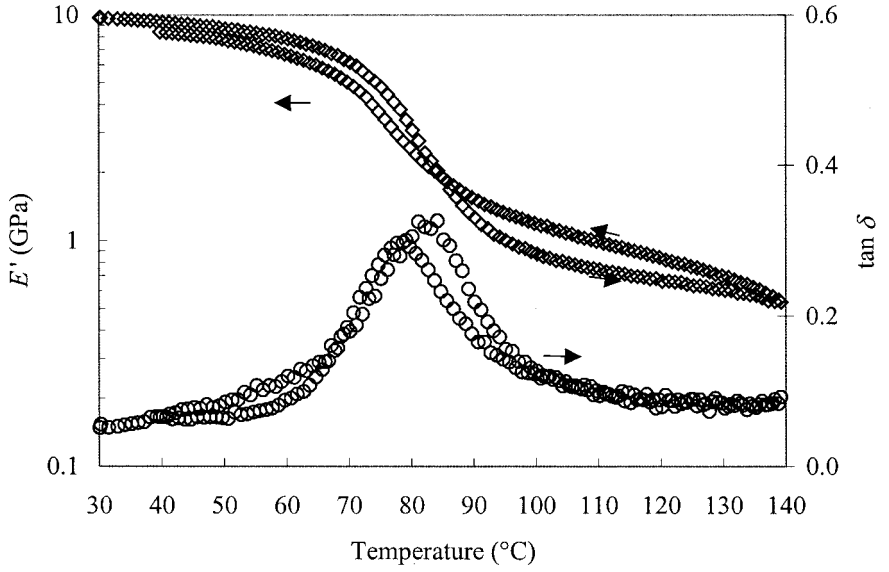

Figure 5 DMTA plot demonstrating the effects of physical aging. The cooling scan shows that E' above T_g is increased by secondary crystallization but decreased below T_g because of the erasure of physical aging.

Measuring the true modulus of fibers can prove difficult; values determined by DMTA as a function of DR are shown in Figure 6. The trends observed are similar to Instron-type test results found in the literature; the modulus increases with DR but drops off at high DRs.[15] The drop-off is attributed to crazing present in fibers that have been highly stressed, weakening the fibers. Traditional tensile tests on fibers are difficult and show a straight line in the stress–strain curve at deformations around 10%, at which point the supramolecular structure is already disrupted. In contrast, the maximum strain is only 0.1% in these DMTA analyses, providing a much more accurate value for the modulus at low deformations. At a 0.1% strain, the fiber morphology is evidently not disrupted.

Tapping-mode AFM images of fibers drawn to DR = 4, 6, and 8 are presented in Figure 7. In each case, the arrow indicates the fiber axis. The morphology is clearly fibrillar. At DR = 4, the microfibrils are not very well defined, and most are not exactly parallel to the fiber axis. At DR = 6, the majority of the microfibrils are aligned with the axis. The only obvious tilt occurs in small sections of each microfibril. Increasing the DR to 8 results in microfibrils that are very straight and regular. Figure 7 represents the structure in the core of the fiber. Microfibrils bundle together to form fibrils, which are approximately a few micrometers in diameter and are visible in an optical microscope.[19,20] In each fibril, there may be thousands of microfibrils.

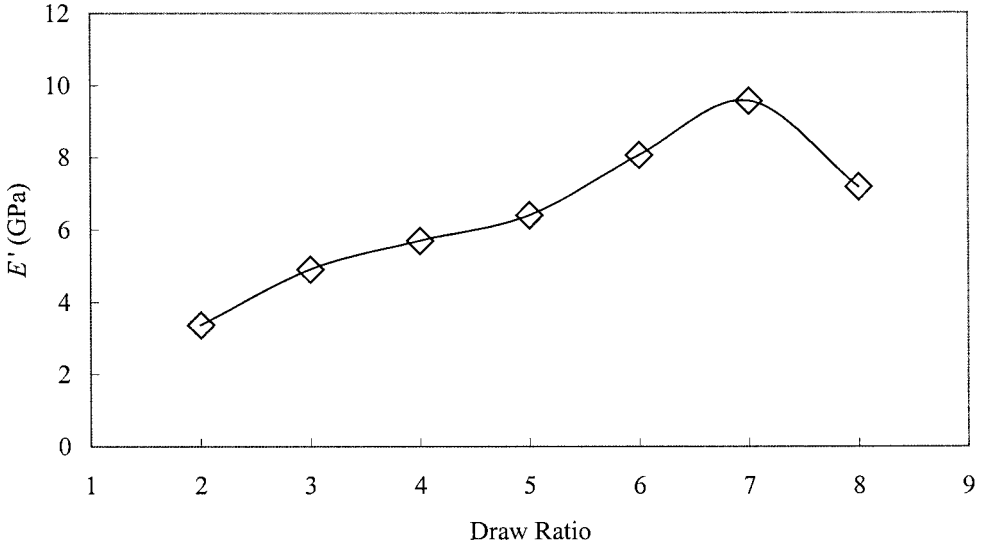

Figure 6 E' versus DR, as determined from DMTA.

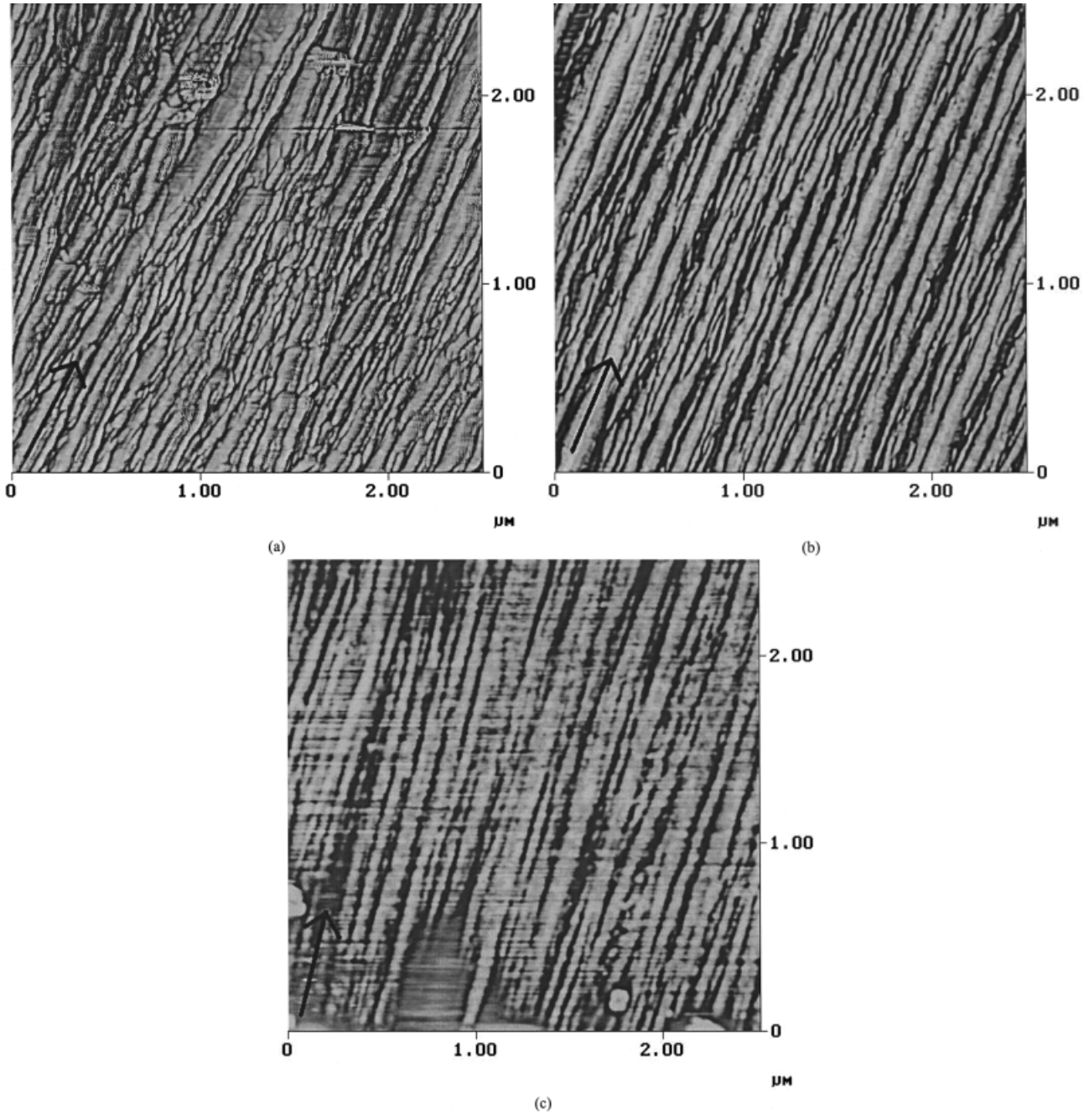

Figure 7 AFM phase images of fibers with DRs of (a) 4, (b) 6, and (c) 8. With increasing DR, the microfibrils become more regular and aligned. The arrows indicate the fiber axis.

The outer surface of a PLA fiber cannot be imaged in exactly the same fashion as the core. A skin, presumably created by high shear forces at the spinneret, envelops the microfibril-laden core. When AFM is used to image the outermost microfibrils (those just underneath the skin), the drive amplitude required to view them is approximately 10 times that needed to image the core. The high driving force is necessary to penetrate the homogeneous skin, which is thought to be approximately 10–100 nm thick.[21]

SAXS patterns of PLA fibers produced at DRs of 3 and 7 are shown in Figure 8. The patterns exhibit so-called void scattering, similar to that observed in Kevlar.[22] Kevlar is known to exhibit fibrillar morphology. The term *void scattering*, although originally intended to describe scattering caused by voids along the axis of a fiber, has become the popular phrase to express all modes of producing equatorially concentrated scattering. The SAXS patterns obtained are consistent with a fibrillar morphology. For low DRs (DR = 3), the equatorial scattering is evident but weak, indicating a small amount of fibrillar development. At high DRs (DR = 7), however, the scattering is highly concentrated in an equatorial streak, revealing the

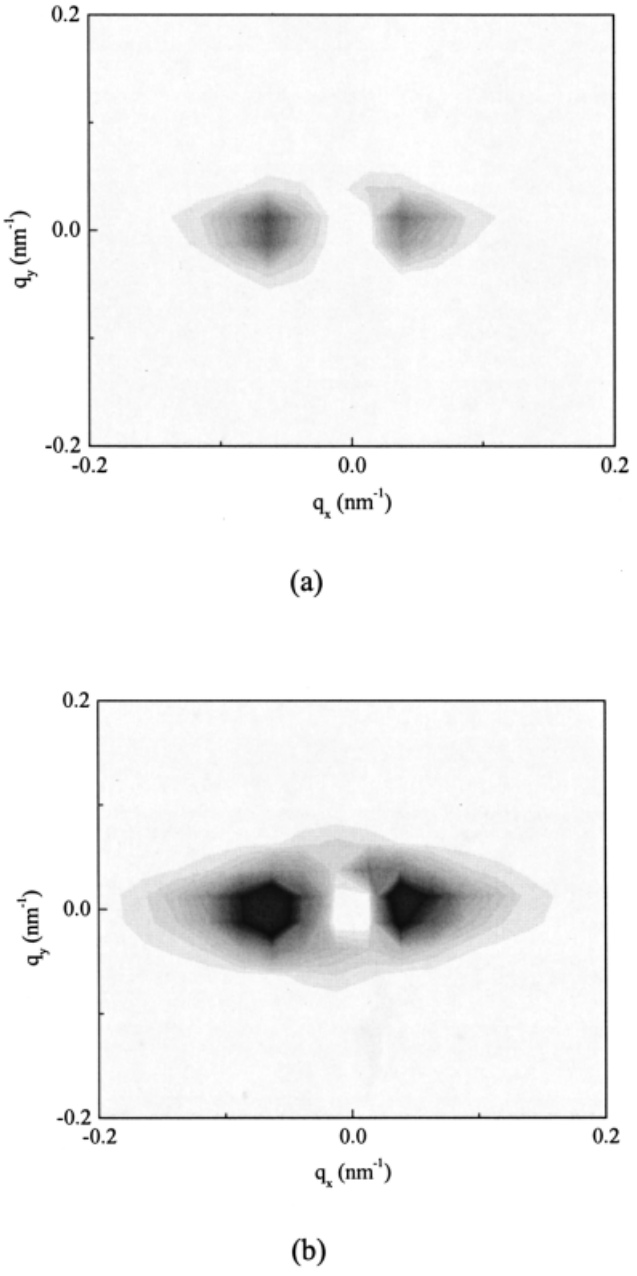

Figure 8 SAXS scattering patterns of fibers with (a) DR = 3 and (b) DR = 7. The equatorial streak, consistent with fibrillar morphology, intensifies as the DR is increased.

presence of a substantial population of microfibrils. Also, in contrast with the DR = 3 fiber pattern, the DR = 7 pattern shows some meridional scattering. The vertical scattering is faint, and the resolution is insufficient to provide a clear indication of any morphological feature. Chu et al.[23] noted the lack of vertical scattering in semicrystalline isotactic polypropylene fibers at high DRs. Although the isotactic polypropylene fibers did show sharp vertical scattering at low DRs, presumably because of lamellae, the PLA fibers studied in this work do not exhibit substantial meridional scattering in any case. The equatorial streak simply intensifies and broadens as DR increases. PLA is known to have low electron-density contrast between amorphous and crystalline regions.[24]

A quantitative assessment of fiber morphology is depicted in Figure 9, a plot of the microfibril diameter versus the DR. The microfibrils are assumed to be closely packed, so that the microfibril diameter is taken as the center-to-center distance. This distance almost doubles between DR = 3 and DR = 8. A plateau of about 42 nm is exhibited for DRs of 4, 5, and 6; however, most mechanical properties undergo a significant change through these DRs.[15]

Lamellae are difficult to view clearly with the AFM technique. Figure 10, an image of a PLA fiber drawn to DR = 5, demonstrates the alignment of lamellae. The lighter spots in the image are areas of higher rigidity in which crystallites are found. The AFM tip does not deform these areas as much as the amorphous regions, which appear as dark spots. The crystallites in one microfibril appear to be aligned adjacent to crystallites in adjacent microfibrils. The lamellar stacks are so prevalent in the image that they are more easily distinguishable than the microfibrils. Furthermore, the lamellae occasionally appear to span over two or more microfibrils, possibly indicating that areas of dense packing of extended interfibrillar tie molecules are being probed. However, the spanning lamellae could instead be artifacts resulting from the AFM tip not accurately following the contours of the microfibrils.

The determination of lamellar thicknesses is difficult because of the scarcity of images demonstrating distinct lamellae. Based on a number of AFM images, rough calculations provide long spacings of about 40 nm. In support of the AFM-derived long spacing of 40 nm, Hoogsteen et al.[12] calculated a long spacing of 50 nm for solution-spun PLA fibers with SAXS.

Larger scale features are also observed in PLA fibers. At high DRs (7 and 8), wavy striations appear perpendicular to the fiber axis, as shown in Figure 11. The microfibrils are not replaced by the striations; the former are still visible. Additionally, the striations are present not only at the surface of the fiber but in the core as well. They could be caused by a draw resonance or elastic instability type of phenomenon. Their period length is roughly 500 nm, corresponding to a frequency of 5×10^6 Hz. The striations are likely a signal of the onset of crazing; the fiber is on the verge of fracturing at such high DRs.

Barham and Keller[25] proposed that two classes of morphological features exist. Class 1 includes features resulting from stress- and flow-induced crystallization and those synthesized as extended chains. Molecules in class 1 materials are first aligned and then crystallized. Class 2 includes materials in which the original crystalline structure is disrupted by solid-state drawing. The molecules are stretched and aligned with the orienting force. Class 1 features essentially retain their

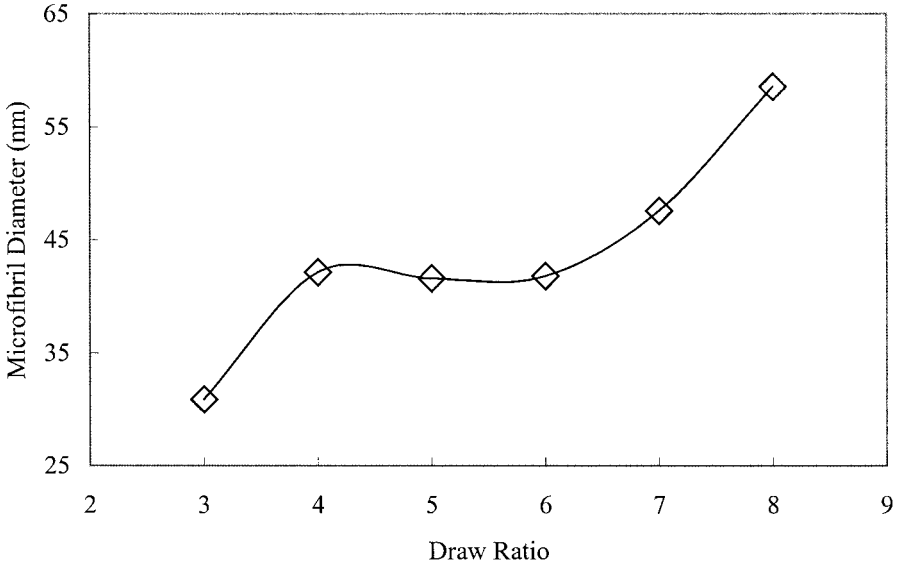

Figure 9 Microfibril diameter as a function of DR. The values nearly double from about 30 nm at DR = 3 to about 60 nm at DR = 8.

dimensions when heated close to, but not above, the melting point. Class 2 materials, however, because the solid-state drawing of the disrupted structure results in significant internal stresses, shrink enough to almost completely reverse the effects of orientation.

A plot of the shrinkage in boiling water is presented in Figure 12. At elevated temperatures, oriented amorphous polymer chains revert toward a random-coil configuration,[10] resulting in the observed shrinkage. Crystals act as anchors and impede the movement of the amorphous molecules. Although the fiber at DR = 2 is completely amorphous, the low stress has not imparted full orientation to the polymer chains, and shrinkage reaches about 50%. Increasing the DR to 3 and 4 induces some crystallization and at the same time extends the amorphous chains. These fibers, containing low crystallinity coupled with greatly extended amorphous chains, shrink up to 60% in boiling water. A transition occurs at DR = 5. Although the

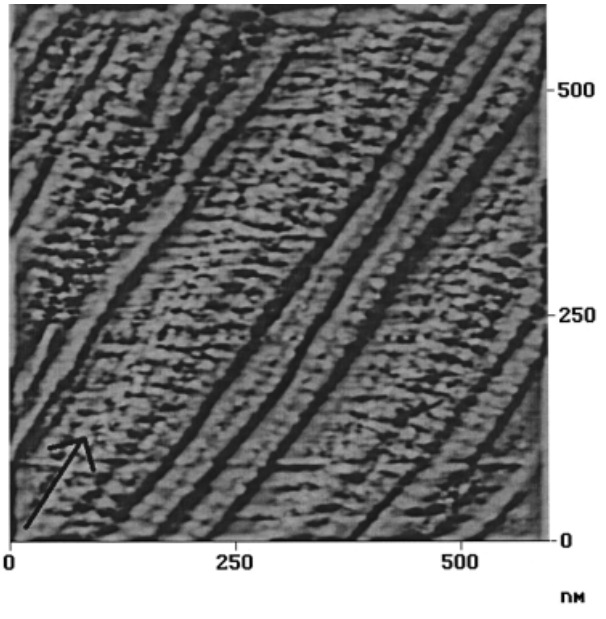

Figure 10 AFM image of lamellar alignment. The lamellae appear as alternating dark and light bands along the microfibrils. Crystalline regions (light areas) in one microfibril are adjacent to crystalline regions in adjacent microfibrils. Some lamellae appear to span multiple microfibrils. The arrow indicates the fiber axis.

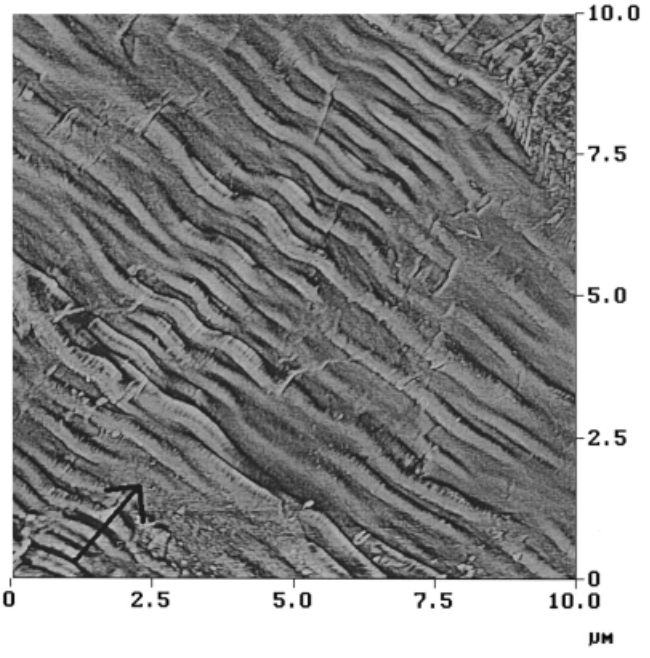

Figure 11 AFM image of a fiber exhibiting wavy striations perpendicular to the axis (indicated by the arrow). Microfibrils are still visible parallel to the axis.

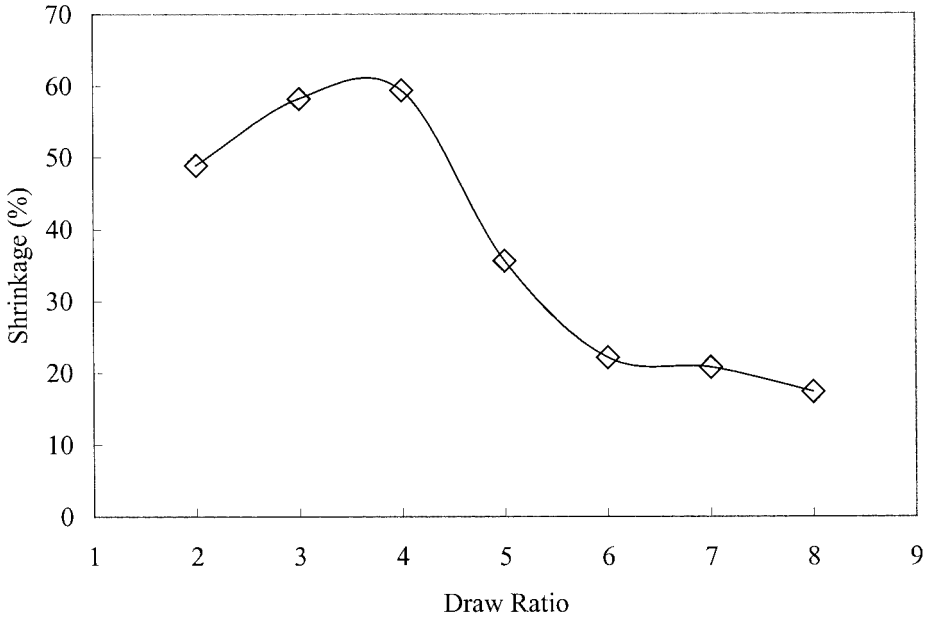

Figure 12 Shrinkage in boiling water versus DR. The transition from high shrinkage to low shrinkage at DR = 5 is thought to reflect the transition from class 2 to class 1.

crystallinity percentages at DR = 3 and DR = 5 are the same, the latter fibers shrink only about two-thirds as much as the former. Given equal crystallinities, one even expects that the DR = 5 fiber will shrink more than the DR = 3 fiber because the amorphous chains are more extended. This exception demonstrates that the crystallinity percentage alone does not dictate shrinkage. The high extent of shrinkage (ca. 60%) seen for DRs of 2, 3, and 4 places these fibers in class 2. The fibers drawn to DR = 6, 7, and 8 shrink very little in boiling water (ca. 20%) and, therefore, belong to class 1.

Figure 13 shows how E' varies with the microfibril diameter. E' exhibits an abrupt change between microfibril sizes of 40 and 45 nm, with values nearly doubling from 5 to over 9 GPa. The loss in E' at large microfibril diameters coincides with the development of crazing in the high-DR fiber. The graph indicates that if the desired property is high modulus, the microfibril size should be greater than 45 nm, whereas the diameter should be less than 40 nm when low modulus is desired (i.e., fabric drape and hand properties are superior when modulus is low). Microfibril diameters less than 40 nm correspond to class 2 be-

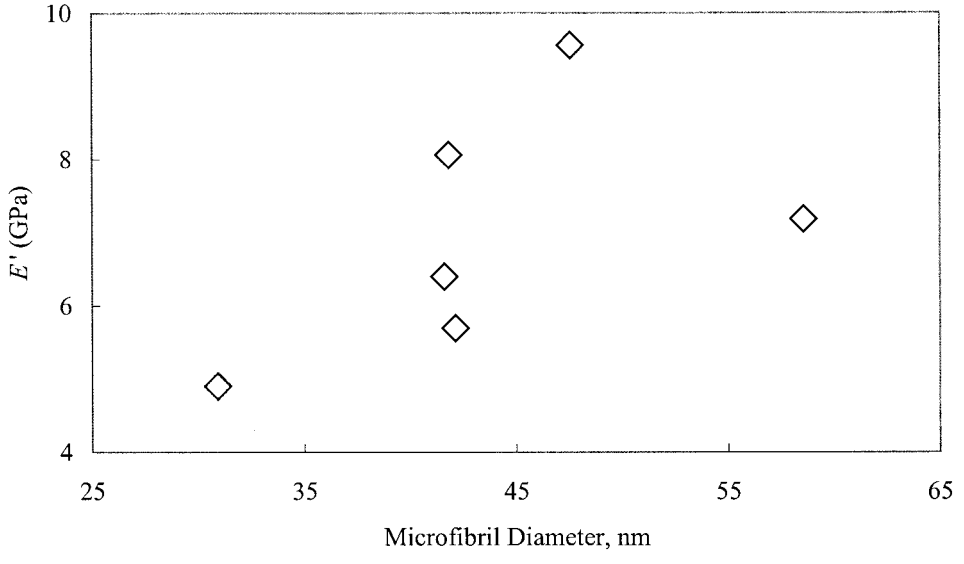

Figure 13 E' determined by DMTA versus microfibril diameter. Below about 42 nm, E' is low (class 2 morphology); above 42 nm, E' is high (class 1 morphology).

havior (lower DRs), whereas larger diameters correspond to class 1 behavior. Mechanical properties are, therefore, not simply dependent on morphological feature size but are highly influenced by class 2 or class 1 formation history.

Prevorsek et al.[26] proposed that microfibrils belong to class 1 and extended-chain interfibrillar molecules belong to class 2. However, the aforementioned shrinkage experiments on PLA fibers, coupled with the confirmed fibrillar morphology present at DRs of 3–7 (and possibly at DR = 2), imply that class 1 and class 2 describe mechanisms rather than actual structural features. It is thought that the low-DR fibers first crystallize in the radiant heating zone and then fibrillate (form fibrils) immediately after exiting the zone, at which point the fibers have cooled down. The fibrillation and drawing disrupt the structure, resulting in substantial internal stresses. These stresses are relaxed at boiling water temperatures, as evidenced by the high degrees of shrinkage. The orienting force during drawing of the high-DR fibers is so great that stress-induced crystallization is simultaneously accompanied by, or preceded by, fibrillation. Because the chains are aligned and then crystallized, internal stresses are much smaller than those of class 2 fibers. Theoretically, these fibers should not shrink in boiling water, but there must be some drawing after crystallization is complete; the fibers do shrink about 20%. This shrinkage may also arise from extended interfibrillar chains.

The transition from class 2 fibers to class 1 fibers essentially reflects the relative rates of fibrillation and crystallization. Class 2 represents crystallization and then fibrillation. Class 1 represents one of two processes: (1) fibrillation and then crystallization or (2) simultaneous fibrillation and crystallization. The transition between the two classes occurs at a DR of 5. The modulus exhibits a jump in value from DR = 5 to DR = 6. Although the microfibril diameters are approximately equal for DRs of 4, 5, and 6, the transition from 60 to 40 to 20% shrinkage emphasizes the fact that shrinkage is not solely due to the amount or size of microfibrils but is also due to the mechanism of morphological development (class 2 vs class 1). One could argue that the crystallinity percentage is responsible for the observed trend. However, crystallinities are equal for DR = 3 and DR = 5, whereas shrinkage values are significantly different.

A complete model for the supramolecular fibrillar morphology in PLA fibers is proposed schematically in Figure 14. The lower inset illustrates the molecular-scale structure in relation to the microfibrils. Within each microfibril, alternating crystalline and amorphous regions are stacked, whereas the interfibrillar area is presumed to be populated by extended but uncrystallized molecules. The model depicted in the inset of Figure 14, in which crystallites in adjacent microfibrils are aligned next to one another, is also thought to represent the structure of melt-spun nylon-6 fibers.[26]

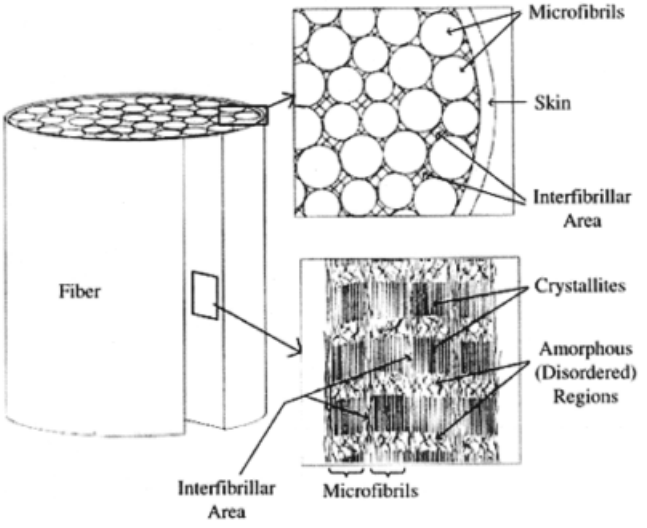

Figure 14 Supramolecular morphological model for two-step, melt-spun PLA. The lateral cross section (upper inset) shows the skin–core morphology, in which the skin is approximately 10–100 nm thick. The longitudinal cross section (lower inset) displays the microfibrillar alignment with crystalline, amorphous, and interfibrillar areas.

The model for the adjacent alignment of crystallites contrasts with that for poly(ethylene terephthalate) (PET), in which the crystallites in adjacent microfibrils are staggered so that crystalline sections of one microfibril are adjacent to amorphous regions of the next.[26] Although one might expect PLA (a polyester) to behave like PET, the fact that both contain an ester linkage does not override more dominating molecular characteristics. PLA and nylon-6 both have fairly flexible molecular backbones and exhibit hydrogen bonding.

CONCLUSIONS

T_g's of two-step, melt-spun PLA fibers increase from 62°C at low DRs to 70°C at high DRs. After months of storage, physical aging results in increased stiffness, as elucidated in DMTA analyses of E'. Thermal and mechanical properties, such as shrinkage in boiling water and modulus, are not solely dictated by the microfibril size or crystallinity percentage alone. The combined effects of stress and temperature influence the crystallinity, alignment, and morphological feature size and type, which, in turn, dictate the properties of the fiber.

With AFM and SAXS, PLA fibers are found to exhibit fibrillar morphology. A model of the supramolecular morphology is proposed. The fibers consist of a skin, approximately 10–100 nm thick, which surrounds a microfibril-populated core. Microfibril diam-

eters range from 30 to 60 nm and increase with DR. Alternating crystalline and amorphous lamellar stacks are indicated by alternating light and dark regions along a number of microfibrils in AFM images.

References

1. Fambri, L.; Pegoretti, A.; Mazzurana, M.; Migliaresi, C. J Mater Sci Mater Med 1994, 5, 679.
2. Gogolewski, S.; Pennings, A. J. J Appl Polym Sci 1983, 28, 1045.
3. Horacek, I.; Kalisek, V. J Appl Polym Sci 1994, 54, 1751.
4. Leenslag, J. W.; Gogolewski, S.; Pennings, A. J. J Appl Polym Sci 1984, 29, 2829.
5. Leenslag, J. W.; Pennings, A. J. Polymer 1987, 28, 1695.
6. Fambri, L.; Pegoretti, A.; Fenner, R.; Incardona, S. D.; Migliaresi, C. Polymer 1997, 38, 79.
7. Eling, B.; Gogolewski, S.; Pennings, A. J. Polymer 1982, 23, 1587.
8. Incardona, S. D.; Fambri, L.; Migliaresi, C. J Mater Sci Mater Med 1996, 7, 387.
9. Schmack, G.; Tandler, B.; Vogel, R.; Beyreuther, R.; Jacobsen, S.; Fritz, H.-G. J Appl Polym Sci 1999, 73, 2785.
10. Mezghani, K.; Spruiell, J. E. J Polym Sci Part B: Polym Phys 1998, 36, 1005.
11. Yuan, X.; Mak, A. F. T.; Kwok, K. W.; Yung, B. K. O.; Yao, K. J Appl Polym Sci 2001, 81, 251.
12. Hoogsteen, W.; Postema, A. R.; Pennings, A. J.; ten Brinke, G.; Zugenmaier, P. Macromolecules 1990, 23, 634.
13. Witzke, D. R. Ph.D. Dissertation, Michigan State University, 1997.
14. Fischer, E. W.; Sterzel, H. J.; Wegner, G. Kolloid Z Z Polym 1973, 980.
15. Cicero, J. A.; Dorgan, J. R. J Polym Environ 2001, 9, 1.
16. Alberola, N.; Cavaille, J. Y.; Perez, J. J Polym Sci Part B: Polym Phys 1990, 28, 569.
17. Hoffman, J. D.; Davis, G. T.; Lauritzen, J. I. Treatise on Solid State Chemistry; Plenum: New York, 1976; Vol. 3.
18. Huang, J.; Lisowski, M. S.; Runt, J.; Hall, E. S.; Kean, R. T.; Buehler, N.; Lin, J. S. Macromolecules 1998, 31, 2593.
19. Van Krevelen, D. W. Properties of Polymers, 3rd ed.; Elsevier: New York, 1990.
20. Neogi, P. Diffusion in Polymers; Marcel Dekker: New York, 1996.
21. Kitagawa, T.; Murase, H.; Yabuki, K. J Polym Sci Part B: Polym Phys 1998, 36, 39.
22. Grubb, D. T.; Prasad, K.; Adams, W. Polymer 1991, 32, 1167.
23. Ran, S.; Zong, X.; Fang, D.; Hsiao, B. S.; Chu, B. Macromolecules 2001, 34, 2569.
24. Runt, J. Pennsylvania State University, personal communication.
25. Barham, P.; Keller, A. J Polym Sci Lett 1975, 13, 197.
26. Prevorsek, D. C.; Kwon, Y. D.; Sharma, R. K. J Mater Sci 1977, 12, 2310.